Random surfaces: from polymer membranes to strings

1994 J. Phys. A: Math. Gen. 27 3323

(http://iopscience.iop.org/0305-4470/27/10/009)

J. Phys. A: Math. Gen. 27 (1994) 3323–3353. Printed in the UK

REVIEW ARTICLE

Random surfaces: from polymer membranes to strings

J F Wheater
Department of Physics, Theoretical Physics, 1 Keble Road, Oxford OX1 3NP, UK

Received 17 June 1993

Abstract. I review the state of knowledge about random surface ensembles in continuous embedding spaces and their possible role in defining strings in arbitrary dimensions. The application of rigorous statistical mechanics, approximate calculation and numerical simulation is described.

1. Introduction

The subject of random surfaces pervades much of theoretical physics. In 1970 Nambu [1] formulated the theory of a one-dimensional object, the string, propagating in spacetime and in so doing sweeping out a two-dimensional object, the world sheet. The interest at that time was in the properties of hadronic elementary particles [2]; many years later strings became fashionable as a theory of everything and Polyakov's quantized string [3] in Euclidean spacetime was reformulated as a problem in the statistical mechanics of random surfaces [4–6]. In 1973 Helfrich [7] was concerned with the membranes which enclose biological cells and sometimes exhibit remarkable fluctuations [8–10]. Subsequently many apparently disparate physical systems have been formulated in terms of the statistical mechanics of two-dimensional surfaces embedded in a space of higher dimension. The boundaries between domains of differently oriented spins in the three-dimensional Ising model are surfaces and the entire partition function can be rewritten as a sum over the domain boundaries rather than the original spins [11]. In three dimensions, the strong-coupling expansion of lattice gauge theories can be written as a sum over surfaces [12] while the large-N limit of $SU(N)$ gauge theories is also related to the string [13]. Apart from biological membranes, there are many real two-dimensional objects in condensed-matter systems, such as the interface between two phases [14], whose connection to surfaces is obvious. In all of these systems not just one particular surface but a whole ensemble of possible surfaces is involved; hence the word 'random' in the title refers to annealed (rather than quenched) randomness.

With such wide-ranging applications it is natural to try to abstract the essential features of the description in terms of random surfaces and to reduce them to a small number of classes. The idea of universality has proved to be a powerful one in statistical physics and ultimately an understanding of the universality classes of random surfaces is our aim. Broadly speaking, random surface models have been formulated in three distinct ways. In the first approach the whole of space is discretized into, for example, a cubic lattice; the surfaces are then built up out of a set of elementary squares, or plaquettes, of the lattice with neighbouring squares in the surface sharing a link of the lattice. These models, sometimes called 'plaquette surfaces', are natural if ones starting point is an Ising model or a lattice gauge theory. In the second approach only the surface itself is discretized, by drawing

0305-4470/94/103323+31$19.50

a two-dimensional lattice upon it, while being allowed to move continuously in three-dimensional space; this formulation is somewhat more natural from the point of view of strings or polymerized membranes. The third approach does not discretize the system at all and deals only with the effective field theories which are supposed to characterize the long-distance properties of the surface. In a sense this approach is derivative in that these models have ultra-violet divergences which need regularizing and often have interesting behaviour at values of their coupling constants too large for perturbation theory to be reliable; the discretized models provide a consistent non-perturbative ultra-violet regularization. In most cases our aim is to discover which continuum effective field theory describes the non-trivial long-distance properties of the surface, if indeed it has any. If universality for surfaces is anything like that for other systems we might expect that the two different discretizations will, provided the models have certain features in common, lead to the same continuum effective field theory.

Even after reducing all the physically interesting systems to a smaller set of models the subject is still too vast to be covered adequately in one short article. This article describes the formulation in which the surface is discretized but the embedding space remains continuous with particular emphasis on its relevance to strings. I have tried to include sufficient detail that it will, I hope, help someone new to the field get started. There are a number of references which provide access to those areas omitted from this article. The situation up to 1989 is well covered in [15] while the closely related subjects of quantum gravity and matrix models are reviewed in [16, 17]. For recent progress on plaquette surfaces see [18] and references therein.

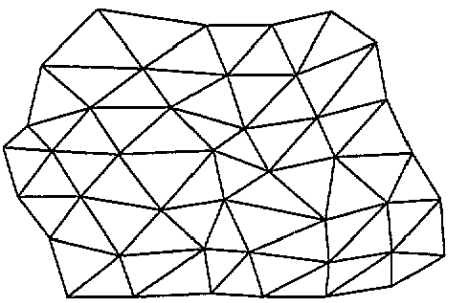

Figure 1. Segment of a crystalline surface.

2. The discretized models

The basic models can be developed in a straightforward way by considering first a thin flexible sheet *in vacuo*. It has thermal partition function

$$Z = \sum_{C} e^{-\beta S} \tag{1}$$

where β is the inverse temperature, S the energy and C represents all configurations of the surface. To specify what the sum over configurations means, a microscopic description of the sheet is useful. Suppose that it is actually made of elastic links (which might be chain molecules) joined together in a fixed regular triangular-lattice pattern (hence the name crystalline surface) as shown in figure 1 and that altogether there are N vertices labelled by $\{i = 1, \ldots, N\}$. The two-component lattice vector $\vec{\xi}_i$ denotes the location of site i relative

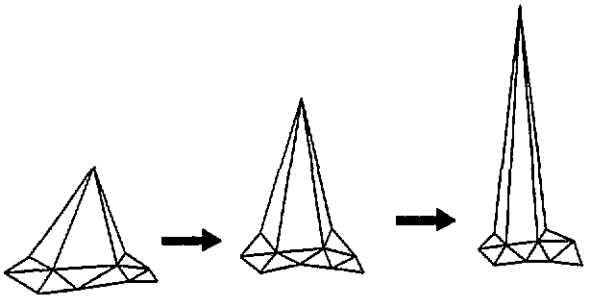

Figure 2. Sequence of configurations of increasing spikyness but constant area.

to some arbitrary fixed site. The configuration of the surface is defined by the position vectors $\{\boldsymbol{X}(\vec{\xi}_i), i = 1, \ldots, N\}$ of the vertices in three-dimensional space; when there is no danger of confusion we will use the abbreviated notation $\boldsymbol{X}(i)$ for $\boldsymbol{X}(\vec{\xi}_i)$. (Sometimes the embedding space has dimension D different from three, in which case $\boldsymbol{X}$ becomes a D-component vector.) Provided the surface is allowed to self-intersect without hindrance (sometimes called a phantom surface) then the sum over configurations is simply given by integrating over all the possible locations of the vertices so

$$\sum_{\mathrm{C}} \to \prod_{i=1}^{N} \int \mathrm{d}^3 \boldsymbol{X}(i)\ \delta^3\left(\sum_{i=1}^{N} \boldsymbol{X}(i)\right). \tag{2}$$

The role of the delta function is to suppress the translational zero mode of the surface.

The simplest contribution to S arises from the elastic energy and it is tempting to write this directly in terms of the surface tension σ as

$$S_0 = \sigma A \tag{3}$$

where A is the area. Such a model has a fundamental problem first discussed by Ambjørn *et al* [4]. Consider the sequence of configurations shown in figure 2; as the spike is pulled further out of the plane its area can be kept fixed by contracting the base. Because there are N sites, for every flat surface of area A there will be N surfaces with one infinite spike, $N(N-1)/2$ with two infinite spikes and so on. The partition function Z is dominated by surfaces with infinite spikes! Ambjørn *et al* gave a rigorous proof that this is so and that, depending on the connectivity of the lattice, either Z itself or its higher moments are infinite even for finite N. According to the picture of a network of chain molecules it is not really surprising that something has gone wrong because the true elastic energy of the system is given not by σA but by

$$S_{\mathrm{G}} = \sum_{\langle ij \rangle} \tfrac{1}{2} l_{ij}^2 \tag{4}$$

where $\langle ij \rangle$ denotes the link running between vertices i and j and l_{ij} its extension (we have scaled the elastic constant to 1 which is always possible, see section 5.1). Now the elastic energy gets very big for the spikey configurations and they are suppressed. It is actually convenient to suppose that the links have zero natural length so that l_{ij} becomes the length of the link and then

$$S_{\mathrm{G}} = \sum_{\langle ij \rangle} \tfrac{1}{2} |\boldsymbol{X}(i) - \boldsymbol{X}(j)|^2 . \tag{5}$$

Now, when all the molecules have much the same length the triangles are almost equilateral and have area $\sim l^2$ so that $S_0 \sim S_G$ and for smooth surfaces we recover the usual macroscopic description in terms of surface tension. An alternative formulation of the elastic energy is the so-called tethered potential [19]. S_G is replaced by

$$S_T = \sum_{\langle ij \rangle} V(l_{ij}) \tag{6}$$

where

$$V(x) = \begin{cases} 0 & \text{if } x < a \\ \infty & \text{if } x > a\,. \end{cases} \tag{7}$$

All the available evidence suggests that S_G and S_T are in the same universality class; however, the former is easier to handle analytically and has a more natural correspondence with the continuum models that we will discuss later.

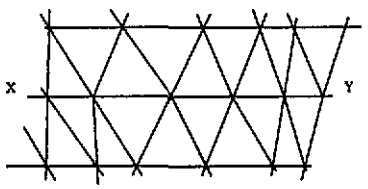

Figure 3. A fold along X–Y does not cost elastic energy.

As it stands, our model still allows some distortions of the surface with no energy cost. For example, the folding of a flat surface along the line X–Y marked in figure 3 does not stretch any links and so does not increase the elastic energy. Now there are many configurations having the same elastic energy but folded up in different ways so the partition function (and hence the physics of the model) is dominated by surfaces which are all folded up—as we will see in section 5.1 the surfaces are crumpled. This can be counteracted by adding an energy which increases as the bending angle increases as would be expected of a real rubber sheet. A simple way of modelling this is to add a contribution to the energy

$$\frac{\kappa}{\beta} S_{ec} \tag{8}$$

where S_{ec} denotes the extrinsic curvature given by

$$S_{ec} = \sum_{\langle ij \rangle} (1 - \hat{n}_\Delta \cdot \hat{n}_{\Delta'}) = \tfrac{1}{2} \sum_{\langle ij \rangle} (\hat{n}_\Delta - \hat{n}_{\Delta'})^2 \tag{9}$$

where $\hat{n}_\Delta, \hat{n}_{\Delta'}$ are the unit normal vectors of the triangles sharing the link $\langle ij \rangle$ [19]. The coupling constant κ is often called the bending rigidity. The more rapidly the direction of the unit normals to the surface changes as we move along the surface, the higher the extrinsic curvature. Thus the role of S_{ec} is to suppress the tendency of the surface to crumple up. There are other ways of writing S_{ec} on a lattice which are at first sight equivalent to (9) when applied to surfaces which are nearly smooth [20, 21]. In some cases it has been shown that when applied to very rough surfaces they suffer from pathologies which prevent them from acting to smooth the surface out [22, 23].

However, there are some modifications which are not manifestly sick but which have not yet been subjected to the same exhaustive study as (9). We do not have space to discuss them here and simply refer the reader to the original references [24, 25]. For the purposes of this article the partition function of the crystalline membrane is defined to be

$$Z^{\mathrm{C}}(\beta,\kappa)=\prod_{i=1}^{N}\int \mathrm{d}^3X(i)\;\delta^3\Big(\sum_{i=1}^{N}X(i)\Big)\exp\left(-\left(\beta S_{\mathrm{G}}+\kappa S_{\mathrm{ec}}\right)\right). \tag{10}$$

The defining difference between a crystalline membrane and a fluid one is that in the latter the links (molecules) are not tied to their neighbours in a fixed pattern but are instead free to move through the surface. A simple way to implement this in an equilibrium statistical mechanics context is to sum over all ways that they can be tied together such that the surface is still a triangulation [4–6]. The partition function for the fluid membrane is given by including a sum over triangulations T in $\sum_C$ so

$$Z^{\mathrm{F}}(\beta,\kappa)=\sum_{T\in T_N}\prod_{i=1}^{N}\int \mathrm{d}^3X(i)\;\delta^3\Big(\sum_{i=1}^{N}X(i)\Big)\exp\left(-\left(\beta S_{\mathrm{G}}+\kappa S_{\mathrm{ec}}\right)\right) \tag{11}$$

where T_N runs over all possible triangulations with N vertices. This model is not necessarily very realistic as a model of real *liquid* membranes (e.g. soap bubbles) because liquids are almost incompressible and S_{G} is apparently inappropriate—although it is really the compressibility of a large sample rather than of an individual molecule that is important. In the context of strings we will show later that it is most natural to consider this model in the grand canonical ensemble for which the partition function is

$$\mathcal{Z}(\mu,\kappa,\beta)=\sum_{N}\mathrm{e}^{-\mu N}\sum_{T\in T_N}\prod_{i=1}^{N}\int \mathrm{d}^3X(i)\;\delta^3\Big(\sum_{i=1}^{N}X(i)\Big)\exp\left(-\left(\beta S_{\mathrm{G}}+\kappa S_{\mathrm{ec}}\right)\right). \tag{12}$$

This model is often called the 'dynamically triangulated random surface' or DTRS.

Although our discussion of the motivation for these models has been based on concrete (albeit simplified) examples there are two aspects which are of the utmost importance in real condensed-matter physics which we have ignored. The first is of course the issue of self-avoidance; although the surface ensembles equivalent to the simplest string models are allowed to self intersect, something drastic will happen to a real membrane when it touches itself and a complicated constraint must then be added to (2) to exclude self-intersecting configurations. We will discuss briefly the differences caused by imposing the self-avoiding constraint. The second aspect is the subject of hexatic ordering [27], and its associated energy, in membranes [28]. This occurs in an intermediate regime when an almost flat crystalline membrane starts to melt; the hexatic phase is one in which there is still long-range order in the *orientation* of links but not in their lengths. Such phenomena have physical meaning when the links themselves represent real molecules (which scatter light for example). To discuss adequately the important subject of hexatic ordering in membranes would need a whole article of its own and from now on we will not consider it.

3. Surfaces, strings and quantum gravity

The crystalline and fluid membrane models with extrinsic curvature are related to strings and to quantum gravity in two-dimensional Euclidean spacetime. A string is a one-dimensional object (as a particle is a zero-dimensional object) which, as time evolves, sweeps out a world sheet (as a particle describes a world line). In Euclidean time this world sheet is just a surface embedded in the space in which the string propagates. A point P on the world sheet is labelled by intrinsic coordinates $\vec{\xi} = (\xi_1, \xi_2)$ and $\{X_\mu(\vec{\xi}), \quad \mu = 1, \ldots, D\}$ describes the position of P in the D-dimensional embedding space. The intrinsic metric tensor $g(\vec{\xi})_{ab}$, $(a, b = 1, 2)$ determines the geodesic distance (i.e. the shortest distance if you are constrained to move on the surface) ds, between two points whose coordinates are $\vec{\xi}$ and $\vec{\xi} + d\vec{\xi}$ through

$$ds^2 = g_{ab} d\xi^a d\xi^b . \tag{13}$$

The quantum theory for the world sheet has a path-integral formulation [3]

$$Z_{\text{string}} = \int Dg \left(\prod_{\mu=1}^{D} DX_\mu \right) e^{-S[g, \partial X]} . \tag{14}$$

The functional integral $\int Dg$ means summing over all configurations of the metric which are *physically inequivalent* so that each included configuration gives a different set of geodesic distances between points on the surface. For the theory to make sense the action must satisfy several constraints. Firstly, translation invariance in the embedding space requires that the action cannot depend upon the absolute location of the surface; hence it can only depend upon derivatives of X and not X itself. Secondly, it must be reparametrization invariant so that changes of variable

$$\vec{\xi} \to \vec{f}(\vec{\xi}) \tag{15}$$

which leave the physical configuration unchanged also leave S unchanged. Thirdly, the resulting quantum field theory in g and X must be renormalizable. Polyakov [29] argued that for a closed surface S must take the form

$$S = \int d^2\xi \sqrt{g} \left(g^{ab} \partial_a X_\mu \partial_b X_\mu + \kappa R_{\text{ext}} \right) \tag{16}$$

where g denotes $\det(g_{ab})$. R_{ext} is the continuum extrinsic curvature of the surface given by

$$g^{ab} \nabla_a \hat{n} \cdot \nabla_b \hat{n} \tag{17}$$

where ∇ is the covariant (with respect to general coordinate transformations (15)) derivative and $\hat{n}$ is the unit-normal vector to the surface. For general D, (17) is summed over the $D - 2$ independent normal vectors.

If we write

$$Z_{\text{string}} = \int Dg \, Z_g \tag{18}$$

with

$$Z_g = \int DX \exp(-S) \tag{19}$$

then it is clear that Z_{g_0}, where g_0 is a fixed constant metric, is related to the partition function of the crystalline membrane (10) by straightforward discretization of the world sheet into a regular triangular lattice; the derivatives $\partial_a X_\mu$ are approximated by nearest-neighbour site differences in X (5) and the covariant derivatives $\nabla_a \hat{n}$ by nearest-neighbour triangle differences in $\hat{n}$ (9). How to deal with non-constant metrics and then with $\int Dg$ is not so clear but a remarkably elegant construction seems to work. In some loose sense it identifies a given triangulation (not, in general, regular) with a particular metric. Consider the triangulation in figure 4, and define the length of a path to be the number of links in the path. The geodesic distance between two points is then the length of the shortest path connecting them. For example, the geodesic distance AB is 3. By changing the linkage of the triangulation we can change the geodesic distance; flipping the link XY to the dashed link changes the distance AB to 4. The basic hypothesis [4–6] is that, in summing over all triangulations, we are summing over all different sets of geodesic distances between points in a manner equivalent to integrating over the continuum metric (earlier a similar construction based on embedding manifolds in a hypercubic lattice of large dimension was proposed by Weingarten [30]). Similarly, the number of points in the discretized version corresponds to the volume of the metric $\int d^2\xi \sqrt{g}$ in the continuum. In integrating over g there is implied a sum over metrics of different volume and hence in the discretized version we should sum over the number of points. Thus it can be argued that the grand canonical partition function of the DTRS (12) is, at least naively, a discretized version of Z_{string}. One can also argue that this model contains a remnant of the reparametrization invariance (15); the sum over triangulations ensures that the resulting physics cannot depend *a priori* on the features of any particular lattice (coordinate system) although it will depend on the existence of the lattices providing an ultra-violet cut-off.

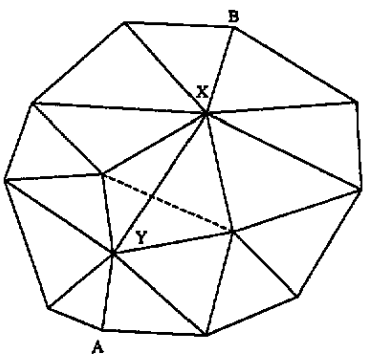

Figure 4. A link flip changes the intrinsic distance AB from 3 to 4.

The partition function (14) may also be interpreted as D bosonic matter fields (the Xs) interacting with two-dimensional quantum gravity (for which the 'universe' is just the surface) in which the dynamical field is the metric g. There is no term in the action involving the metric alone because the two-dimensional equivalent of the Einstein action which describes general relativity in four dimensions is actually a topological invariant proportional to the Euler characteristic of the surface. In the case of conformal matter a great deal is understood about models of this type. The crucial quantity is the central charge c, the number of free (meaning not interacting with themselves, only with gravity) bosonic matter fields in the model. It is possible to construct models with many different, not necessarily integer, values of c and consider their interactions with gravity. For $c \leqslant 1$

the effects of the interaction with gravity can be computed through the famous result of Knizhnik *et al* [31] (hereafter referred to as the KPZ result) and the model with $\kappa = 0$ and $D = 25$ is known to be consistently quantizable. However, for other $c > 1$ the KPZ result breaks down and makes nonsensical predictions which seem to imply that no smooth long-range behaviour is possible. At $\kappa = 0$ the crystalline surface has D independent fields and so $c = D$; as we will see later, the DTRS does not lead to a well defined smooth surface but one which is highly irregular on the scale of the lattice spacing. At $\kappa > 0$ the extrinsic curvature acts to suppress the irregular surfaces and the hope is that this model offers a way round the KPZ result and actually yields smooth continuum surfaces in embedding dimensions $D > 1$.

4. Long distance behaviour and the continuum limit

As we have seen, the lattice models are certainly discretizations of the continuum systems and therefore provide an ultra-violet regularization which goes beyond perturbation theory. However it does not necessarily follow that, by studying the lattice model, we can find out about the continuum one. The difficulty lies in the procedure by which we take the limit where the lattice spacing $a \to 0$. Let us first discuss this for a crystalline surface on which we consider the correlation function G of some local field (i.e. X) dependant quantity $\phi(\vec{\xi}_i)$

$$G = \langle \phi(\xi, 0)\phi(0, 0) \rangle . \tag{20}$$

Typically G shows exponential fall-off with distance

$$G \sim \exp(-m\xi) \tag{21}$$

where m, the mass, is the inverse correlation length in lattice spacings. Introducing the lattice spacing a we can write

$$G \sim \exp\left(-(ma^{-1})(\xi a)\right) = \exp\left(-m_{\text{phys}}\xi_{\text{phys}}\right) . \tag{22}$$

The physical intrinsic distance between the points $(0, 0)$ and $(\xi, 0)$ is $\xi_{\text{phys}} = \xi a$ and the physical mass $m_{\text{phys}} = ma^{-1}$. In taking the continuum limit we want to study successive approximations to G at fixed ξ_{phys} as the lattice spacing $a \to 0$; in order for G to remain finite in this limit it is necessary that $m_{\text{phys}} \to$ constant and hence that $m = m_{\text{phys}}a \to 0$. However, to get $m \to 0$ there must be a second-order phase transition and it is a highly non-trivial matter whether the lattice model has such a transition. If it does not then the approximations made to the continuum model to get the lattice version have been too crude (as is in fact the case with several lattice versions of surfaces with extrinsic curvature [22, 23]). Even if there is a second-order phase transition it does not follow that the effective continuum field theory is that naively obtained from the lattice model by doing an expansion in powers of a and retaining the leading terms in the $a \to 0$ limit.

In considering the DTRS there is one essential difference. The sum over all triangulations means there is no sense in a correlation function of the form (20) because there is no fixed geometrical relationship between the two points. Instead, correlation functions are defined by considering surfaces *with boundaries*. For example a one-point function is given by summing over all surfaces with a single boundary γ fixed in the embedding space

as shown in figure 5 where we have chosen the boundary to be a circle. Formally we have

$$G(\gamma_1) = \sum_N e^{-\mu N} \sum_{T_N:\partial T=\gamma} \prod_{i=1}^{N+n-1} d^3X(i)\, C(X(1),\ldots,X(n)) \exp(-(\beta S_G + \kappa S_{ec})) \quad (23)$$

where the sum over triangulations is now over those with a boundary γ and the constraint C fixes the n points lying on γ to fixed positions in the embedding space. Letting A be the area in lattice units of the circle enclosed by the boundary, σ be the string tension (surface tension) and a be the lattice spacing we expect that

$$G_1 \sim \exp(-\sigma A) = \exp\left(-(\sigma a^{-2})(Aa^2)\right) = \exp\left(-\sigma_{phys} A_{phys}\right). \quad (24)$$

In the continuum limit $a \to 0$ we need σ_{phys} to remain finite and hence $\sigma = \sigma_{phys} a^2 \to 0$. The two-point function is given by summing over all surfaces with two fixed boundaries γ_1 and γ_2 as shown in figure 6. It is usually convenient to shrink γ_1 and γ_2 to points a distance L (in the embedding space) apart for which we get†

$$G_2 \sim \exp(-mL) = \exp\left(-(ma^{-1})(La)\right) = \exp\left(-m_{phys} L_{phys}\right). \quad (25)$$

In the continuum limit $a \to 0$ we need m_{phys} to remain finite and hence $m = m_{phys} a \to 0$. Note that to get a sensible continuum limit it is not enough to have $\sigma, m \to 0$ at a critical point but they must do so keeping the ratio $\sigma_{phys}/m_{phys}^2 = \sigma/m^2$ constant.

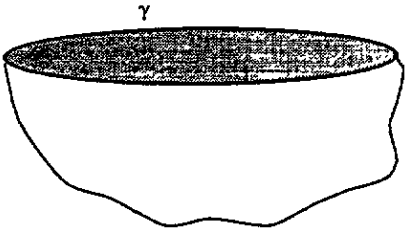

Figure 5. A one boundary surface.

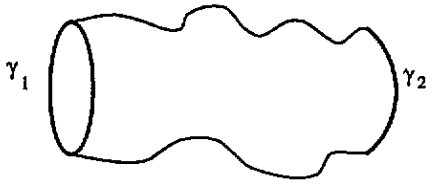

Figure 6. A two boundary surface.

Understanding the phase structure of these models is crucial to determining the effective field theory that governs any non-trivial long-distance behaviour. The rest of this article addresses in turn the following two questions.

(1) Does the crystalline surface have a second-order phase transition and if so what is the corresponding continuum field theory, F_1? If F_1 is a conformal field theory is its central charge greater than one?

(2) Does the dynamically triangulated model also have a second-order phase transition and, if so, is the continuum field theory describing the critical point equivalent to F_1 interacting with gravity analogous to the way that the KPZ result describes this interaction when $c \leqslant 1$?

† Although the symbol m is used for the mass gap in both models, the quantities are unrelated; which one is meant will always be clear from the context.

5. The crystalline surface

5.1. Special cases

As we discussed in section 2, and generalizing to D embedding dimensions for the moment, the partition function for a crystalline random surface is given by

$$Z(\beta,\ \kappa) = \prod_{i=1}^{N} \int \mathrm{d}^D \boldsymbol{X}(i)\, \delta^D\left(\sum_{i=1}^{N} \boldsymbol{X}(i)\right) \exp\{-\beta\, S_{\mathrm{G}} - \kappa\, S_{\mathrm{ec}}\} \tag{26}$$

and expectation values are given by

$$\langle \mathcal{O} \rangle = \frac{1}{Z} \prod_{i=1}^{N} \int \mathrm{d}^D \boldsymbol{X}(i)\, \delta^D\left(\sum_{i=1}^{N} \boldsymbol{X}(i)\right) \mathcal{O}(\{\boldsymbol{X}\})\, \exp\{-\beta\, S_{\mathrm{G}} - \kappa\, S_{\mathrm{ec}}\}\,. \tag{27}$$

The expectation values of some quantities can be calculated exactly for all values of κ because the extrinsic curvature is invariant under the global rescaling

$$\boldsymbol{X}(i) \to \beta^{-1/2} \boldsymbol{X}(i) \qquad \forall i\,. \tag{28}$$

Making this rescaling in (26) gives

$$Z(\beta, \kappa) = \beta^{-(N-1)D/2} Z(1, \kappa) \tag{29}$$

and, therefore,

$$\begin{aligned} \langle S_{\mathrm{G}} \rangle &= -\frac{\partial}{\partial \beta} \ln Z(\beta,\ \kappa) = \frac{(N-1)D}{2\beta} \\ \langle S_{\mathrm{G}}^2 \rangle_c &\equiv \langle S_{\mathrm{G}}^2 \rangle - \langle S_{\mathrm{G}} \rangle^2 = \frac{(N-1)D}{2\beta^2} \end{aligned} \tag{30}$$

and so on. For approximately regular surfaces we argued in section 2 that

$$\langle S_{\mathrm{G}} \rangle \sim \langle A \rangle \tag{31}$$

so that the average area of the surface in units of lattice spacing squared is proportional to the number of points in the lattice. Note that in the limit $N \to \infty$ the ensemble becomes almost microcanonical in that

$$\frac{\langle A^2 \rangle}{\langle A \rangle^2} \sim \frac{1}{N} \tag{32}$$

and the fluctuations in the area become less and less important; this motivates an analytical approximation that we will look at later.

At $\kappa = 0$ the model is of course exactly soluble. $\boldsymbol{X}$ has the two-point function

$$\langle \boldsymbol{X}(i) \cdot \boldsymbol{X}(j) \rangle \sim \sum_{\vec{k}}{}' \frac{1}{L(\vec{k})}\, \mathrm{e}^{\mathrm{i}\vec{k}\cdot(\vec{\xi}_i - \vec{\xi}_j)} \tag{33}$$

where $L(\vec{k})$ denotes the lattice Laplacian in momentum space and the sum runs over all lattice momenta $\vec{k}$ except (0, 0) (so that the δ-function constraint is satisfied). The simplest measure of the shape of the surface is given by the mean-square radius, often called the gyration radius squared,

$$R_g^2 = \frac{1}{N}\sum_{i=1}^{N}\langle \boldsymbol{X}(i)\cdot\boldsymbol{X}(i)\rangle = \sum_{\vec{k}}{}' \frac{1}{L(\vec{k})}. \tag{34}$$

When the number of points N is very large we can replace the sum by the corresponding integral and use $1/\sqrt{N}$ for the lowest allowed momentum to find

$$R_g^2 \sim \int_{1/\sqrt{N}} \frac{d^2k}{k^2} \sim \log N. \tag{35}$$

It is convenient to introduce an exponent, commonly called d_H or the Hausdorff dimension, such that

$$R_g^2 \sim N^{2/d_H} \sim A^{2/d_H}. \tag{36}$$

In this case we have $d_H = \infty$. Now $d_H = 2$ is the behaviour expected of a smooth surface—consider the surface of a sphere for example. As d_H increases the surface becomes more and more convoluted until at $d_H = \infty$ it is space-filling in any embedding dimension—it looks like a very crumpled up sheet of paper. So at $\kappa = 0$ the model is very far from being one of smooth surfaces as the dominant configurations are all crumpled on the shortest available distance scale. What happens as κ increases? The model is no longer analytically solvable and there are three ways forward. The first is by rigorous statistical mechanics methods, the second by approximate continuum calculations and the third by numerical simulation. All yield some insights into the properties of the system and we consider them in turn.

5.2. A toy model

A very simple model which has some of the properties of the crystalline surface was suggested by David and Guitter [28]. Consider a square $L \times L$ lattice in embedding dimension $D = 2$. The elementary squares of the lattice are rigid so that the only possible changes are folds along the lines of the lattice grid. For a given configuration, suppose we do all the folds along one direction followed by those along the other. Each fold costs κL in energy so the partition function is

$$Z = \left(\sum_{n=0}^{L}\binom{L}{k}e^{-\kappa L n}\right)^2 = (1+e^{-\kappa L})^{2L}. \tag{37}$$

If $\kappa > 0$, then for large L

$$Z \simeq 1 + 2Le^{-\kappa L} \tag{38}$$

and $Z \to 1$ as $L \to \infty$; only the unfolded configuration counts and the surface is smooth. At $\kappa = 0$

$$Z = 2^{2L} \tag{39}$$

and all the configurations contribute equally. We see that there is a phase transition at $\kappa = 0$. It is straightforward to calculate the expected number of folds in each direction

$$\langle n \rangle = \begin{cases} L/2 & \kappa = 0 \\ 0 & \kappa > 0 \\ L & \kappa < 0. \end{cases} \tag{40}$$

When $\kappa > 0$ the mean-square extent is proportional to L^2 so $d_H = 2$. At $\kappa = 0$ the folds in one direction are just a one-dimensional random walk so the mean linear extent is $O(\sqrt{L})$ and $d_H = 4$ at the critical point. When $\kappa < 0$, every possible fold is made and the mean-square extent is 1.

One problem with the above model is that the total number of configurations is low; indeed the average entropy per site $2L \log 2/L^2$ is zero. This defect is remedied in a similar model based on a triangular lattice which was proposed by Kantor and Jaric [32]; however, this model still yields a phase transition at $\kappa = 0$.

5.3. Some rigorous results

Jonsson [33] has proved using a variant of the classic Mermin–Wagner argument that, for all κ, $\langle X^2 \rangle \geqslant \log N$ so the surface can never be more crumpled up than its $\kappa = 0$ state—a result which is intuitively obvious but nice to be able to prove. At very large κ we expect to find that folds and crumples are suppressed in the partition function. However, there is no real proof that $d_H = 2$ at large κ. Fortunately, numerical simulations provide incontrovertible evidence that this is the case so it makes sense to enquire about the intermediate behaviour. It turns out that by considering the behaviour of the tangent–tangent correlation functions we can categorize the possible behaviours quite strictly [26, 22]. The treatment described here follows the latter reference.

Suppose that the lattice has periodic boundary conditions with period L where $L^2 = N$, define the tangent vector

$$t_1(\vec{\xi}) \equiv t_1(\xi_1, \xi_2) = X(\xi_1 + 1, \xi_2) - X(\xi_1, \xi_2) \tag{41}$$

and introduce the tangent–tangent correlation function

$$G_{\parallel}(\xi, \xi_2) = \langle t_1(0, \xi_2) \cdot t_1(\xi, \xi_2) \rangle . \tag{42}$$

So long as the ensemble is Euclidean invariant, $G_{\parallel}$ is independent of ξ_2 which we set to zero. As we will show $G_{\parallel}$ has behaviour which is closely related to the long-distance properties of the surface.

It is useful to introduce a definition of the mean-square radius which differs slightly from (34),

$$R_g^2 = \langle |X(L/2, 0) - X(0, 0)|^2 \rangle . \tag{43}$$

Then $G_{\parallel}$ is related to it through

$$R_g^2 = \sum_{\xi=0}^{L/2} \sum_{\xi'=0}^{L/2} \langle t_1(\xi, 0) \cdot t_1(\xi', 0) \rangle = \sum_{\xi=0}^{L/2} \sum_{\xi'=0}^{L/2} G_{\parallel}(\xi - \xi', 0) . \tag{44}$$

The periodic boundary conditions imply a constraint on $G_\parallel$ because the sum of tangent vectors round a closed loop is zero; this gives

$$\sum_{\xi=0}^{L-1} G_\parallel(\xi, 0) = 0 . \tag{45}$$

This constraint implies that $G_\parallel$ must be negative for some values of its argument. We know that $G_\parallel$ takes its maximum value at $\vec{\xi} = 0$ since $\langle t_1(\vec{\xi}) \cdot t_1(\vec{\xi}\,')\rangle \leqslant \langle t_1(\vec{\xi}) \cdot t_1(\vec{\xi})\rangle$ and from (30) that this maximum value is $O(1)$. We therefore make the plausible assumption that $G_\parallel(\xi, 0)$ falls from its maximum value at $\xi = 0$, that it goes negative at $\xi = \xi_0$ and remains negative until $\xi = L - \xi_0$ when it becomes positive again (this assumption is borne out by the numerical simulations). Assuming that the system has only one relevant distance scale we expect that

$$\xi_o \propto m^{-1} \tag{46}$$

where m was introduced in (21). We can distinguish a number of cases.

(1) $G_\parallel(\xi, 0) > 0$ for $\xi < \xi_0$ where ξ_0 is independent of the system size L. Then for arbitrary system size we have

$$\sum_{-\xi_0}^{\xi_0} G_\parallel(\xi, 0) < E \tag{47}$$

where E is a constant independent of L. It then follows that

$$\left| \sum_{\xi_0}^{L-\xi_0} G_\parallel(\xi, 0) \right| < E . \tag{48}$$

For large enough L and $\xi_0 \ll \xi \ll L - \xi_0$ this forces the slowest permissible fall off of $G_\parallel$ to be

$$G_\parallel(\xi, 0) \approx -E'(\xi^{-2+\epsilon} + (L - \xi)^{-2+\epsilon}) \tag{49}$$

where E' is another constant independent of L and $\epsilon < 1$. Combining (44), (47) and (49) then gives

$$R_g^2 \approx 2E\xi_0 + \text{const}\left(\frac{L}{2}\right)^{\epsilon} \tag{50}$$

or that $d_H = 4/\epsilon$. As we have already mentioned, $R_g^2 > \text{const} \log(L)$, so that in fact the range of ϵ is limited to $1 > \epsilon \geqslant 0$.

(2) $G_\parallel(\xi, 0) > 0$ for $\xi < \xi_0$ where $\xi_0 \sim L^{1-\eta}$ with $1 \geqslant \eta \geqslant 0$. Note that $\eta < 0$ is not possible because for large enough L there would be no region in which $G_\parallel < 0$ and (45) would be violated. Similarly $\eta > 1$ forces all $G_\parallel(\xi > 0, 0)$ to be negative for large enough L which is essentially the previous case with $\xi_0 = 1$. We take $\eta = 1$ to mean $\xi_0 \sim \log L$. Now we have

$$\sum_{-\xi_0}^{\xi_0} G_\parallel(\xi, 0) < FL^{1-\eta} \tag{51}$$

where F is a constant independent of L. It then follows that

$$\left| \sum_{\xi_0}^{L-\xi_0} G_{\|}(\xi, 0) \right| < FL^{1-\eta}. \tag{52}$$

For large enough L and $\xi_0 \ll \xi \ll L - \xi_0$ this forces the fall off of $G_{\|}$ to be

$$G_{\|}(\xi, 0) \approx -F'(\xi^{-\eta} + (L - \xi)^{-\eta}) \tag{53}$$

where F' is another constant independent of L. Combining (44), (51), (53) then gives

$$R_g^2 \approx 2FL^{2-2\eta} + \text{const}\left(\frac{L}{2}\right)^{2-\eta} \tag{54}$$

so that $d_H = 4/(2 - \eta)$. Thus for $\eta = 1$ we have $d_H = 4$ and as η decreases to 0, d_H decreases to 2.

At $\kappa = 0$, $G_{\|}$ can be calculated and shows the behaviour discussed in (1) above with $\xi_0 \approx 1$. The extrinsic curvature term in the action tends to smooth the surface so as κ increases we expect that ξ_0 will increase too. There are then two possibilities [26].

(a) ξ_0 satisfies (1) and remains finite for all $\kappa < \infty$. In this case $d_H = \infty$ for all κ and *there is no phase transition.*
(b) At some coupling $\kappa = \kappa_c$ the behaviour of ξ_0 changes to that described in (2) above. There is a phase transition and d_H jumps to a value in the range $2 \leqslant d_H \leqslant 4$. There are three ways this can happen.

(i) d_H jumps to $2 < d_H \leqslant 4$ at $\kappa = \kappa_c$ then continuously evolves to $d_H = 2$ at $\kappa = \infty$.
(ii) $2 < d_H \leqslant 4$ at $\kappa = \kappa_c$ and $d_H = 2$ for $\kappa > \kappa_c$.
(iii) $d_H = 2$ for $\kappa \geqslant \kappa_c$.

Numerical simulations (see section 5.5) strongly suggest that there *is* a continuous phase transition and that for $\kappa > \kappa_c$, $d_H = 2$. There is no evidence that $d_H \neq 2$ at $\kappa = \kappa_c$ but analytic approximations [28, 32], which are decribed in the next section, favour (ii) with $d_H \sim 3$ at $\kappa = \kappa_c$ for surfaces in three dimensions.

5.4. A continuum approximation

The non-polynomial nature of the lattice curvature action makes the model very difficult to handle analytically. However, the observation we made in section 5.1 that, as the lattice size $N \to \infty$, the ensemble is dominated by configurations of fixed area allows us to construct a continuum model which at least looks similar and can be used as the basis of analytic approximations. Define the coordinate system of the surface so that $\partial_1 \boldsymbol{X}$ and $\partial_2 \boldsymbol{X}$ are mutually perpendicular unit tangent vectors

$$\partial_a \boldsymbol{X} \cdot \partial_b \boldsymbol{X} = \delta_{ab}. \tag{55}$$

It follows from this that the normal vector

$$\hat{\boldsymbol{n}} = \partial_1 \boldsymbol{X} \times \partial_2 \boldsymbol{X} \tag{56}$$

is also a unit vector so the extrinsic curvature can be written

$$\int \mathrm{d}^2\xi\, \partial_a \hat{\boldsymbol{n}} \cdot \partial_a \hat{\boldsymbol{n}} \tag{57}$$

which, by liberal application of (55) and integration by parts, reduces to

$$\int \mathrm{d}^2\xi\, \partial^2 \boldsymbol{X} \cdot \partial^2 \boldsymbol{X}\,. \tag{58}$$

Thus we may consider the partition function [28]

$$Z = \int \mathrm{D}\boldsymbol{X}\, \mathrm{D}\lambda\, \exp\left\{-\int \mathrm{d}^2\xi\, \left(\frac{\kappa}{2}\partial^2 \boldsymbol{X} \cdot \partial^2 \boldsymbol{X} - \lambda_{ab}(\partial_a \boldsymbol{X} \cdot \partial_b \boldsymbol{X} - \delta_{ab})\right)\right\} \tag{59}$$

where the Lagrange multiplier field λ is introduced to impose the constraint (55). An ordinary perturbation expansion for this model does not exist but it is possible to do a large D expansion for which purpose we rewrite $\kappa = D\kappa'$ and $\lambda = D\lambda'$. Then

$$Z = \int \mathrm{D}\boldsymbol{X}\, \mathrm{D}\lambda'\, \exp\left\{-D\int \mathrm{d}^2\xi\, \left(\tfrac{1}{2}\boldsymbol{X} \cdot (\kappa'\partial^4 - 2\partial_a \lambda'_{ab}\partial_b)\boldsymbol{X} + \lambda'_{ab}\delta_{ab}\right)\right\}. \tag{60}$$

Integrating out the $\boldsymbol{X}$ field yields

$$\begin{aligned} Z &= \int \mathrm{D}\lambda'\, \exp\left\{-D\left(\tfrac{1}{2}\mathrm{Tr}\log(\kappa'\partial^4 - 2\partial_a\lambda'_{ab}\partial_b) - \int \mathrm{d}^2\xi\, \lambda'_{ab}\delta_{ab}\right)\right\} \\ &= \int \mathrm{D}\lambda'\, \exp -DS_{\mathrm{eff}}(\lambda')\,. \end{aligned} \tag{61}$$

In the $D \to \infty$ limit we can now do a saddle-point calculation, looking for a constant solution for λ' which minimises $S_{\mathrm{eff}}(\lambda')$ and then examining fluctuations about that solution. For constant λ' the effective Lagrangian is simply

$$-\lambda'_{ab}\delta_{ab} + \frac{1}{2}\int \frac{\mathrm{d}^2 p}{(2\pi)^2}\, \log(\kappa' p^4 + 2\lambda'_{ab} p_a p_b) \tag{62}$$

so the saddle-point equation is

$$\frac{1}{2}\int \frac{\mathrm{d}^2 p}{(2\pi)^2}\, \frac{2p_a p_b}{\kappa' p^4 + 2\lambda^0_{ab} p_a p_b} = \delta_{ab} \tag{63}$$

from which it is easy to show that

$$\lambda^0_{ab} = \frac{\kappa'}{2}\delta_{ab} m^2 \qquad m^2 = \Lambda^2 \mathrm{e}^{-8\pi\kappa'/D} \tag{64}$$

where Λ is the ultraviolet cut-off in the momentum integral. Expanding about this non-trivial saddle point by putting

$$\lambda'_{ab} = \lambda^0_{ab} + \tilde{\lambda}_{ab} \tag{65}$$

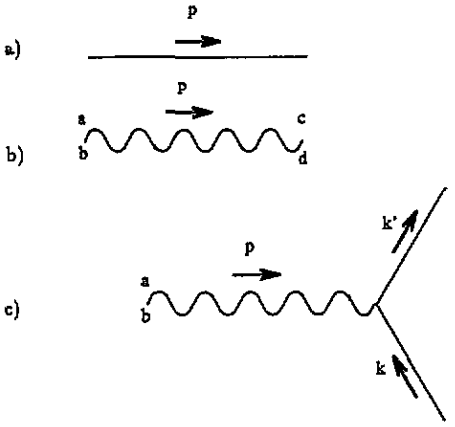

Figure 7. Feynman rules for the action (60) expanded about the saddle point (64).

leads to a sensible perturbation expansion in powers of D^{-1}. The Feynman diagrams for this expansion are made up of three elements.

(i) The X propagator figure 7(a) given by

$$\frac{1}{\kappa'(p^4 + m^2 p^2)}. \tag{66a}$$

(ii) The propagator for the 'phonon' field $\tilde{\lambda}$, figure 7(b)

$$-\frac{8\pi}{3D}\kappa'^2 p^2 \left(\epsilon^{ae}\epsilon^{bf}\frac{p_e p_f}{p^2}\epsilon^{cg}\epsilon^{dh}\frac{p_g p_h}{p^2}\right) + O\left(\frac{p^2}{\log p^2}\right). \tag{66b}$$

(iii) The vertex, figure 7(c),

$$-(k_a k'_b + k_b k'_a). \tag{66c}$$

This theory is renormalizable by power counting and has the important feature that the $\tilde{\lambda}$ propagator has a long-range component no matter what the value of κ'.

The calculation of the renormalization group β function including $1/D$ corrections requires the evaluation of two loop diagrams and is given in [28, 34]. The renormalization group β function for the coupling $\alpha = 1/\kappa'$ is given by

$$\beta(\alpha) = \frac{2}{D}\alpha - \left(\frac{1}{4\pi} + \frac{\text{const}}{D}\right)\alpha^2 + O\left(\frac{1}{D^2}\right). \tag{67}$$

Thus at $D = \infty$ there is only one zero of the β function, at $\alpha = 0$, and at large distance scales the effective inverse rigidity flows to infinity. The structure of the surface is always controlled by the $\alpha = \infty$ ($\kappa' = 0$) fixed point and it is always crumpled. By contrast at finite D the β function has an extra zero at $\alpha^* = 8\pi/D$. When $\alpha > \alpha^*$ the coupling flows towards $\alpha = \infty$ at large distance scales and the surface is crumpled. However, when $\alpha < \alpha^*$ it now flows towards $\alpha = 0$ ($\kappa' = \infty$) and at large distance scales the surface is smooth. At $\alpha = \alpha^*$ there is a second-order crumpling transition and precisely at the transition the membrane has $d_H = 2D/(D-1)$ at first order in $1/D$. The existence of a smooth phase implies the spontaneous breaking of the $O(D)$ invariance of the action (59)

at the phase transition in apparent contradiction of the Mermin–Wagner theorem. However, the long-range component of the phonon propagator which occurs *for all* κ' invalidates the Mermin–Wagner proof. The results of these calculations are perfectly consistent with the general arguments of section 5.3.

An alternative approach to the problem is described by Le Doussal and Radzihovsky [35]. They use a self-consistent screening approximation to calculate the properties of a surface in the smooth regime where at first approximation it is flat and corrections arise from out-of-plane fluctuations. For $D = 3$ they find that $d_H = 2.73$ which is close to the David and Guitter result. Interestingly this approach also allows the calculation of the upper critical dimension $D_{uc} \sim 4.98$ above which the imposition of a self-avoidance constraint does not affect the crumpling transition.

5.5. Numerical simulation

We have seen that some features of the crystalline random surface can be understood analytically. Nonetheless, most of the central questions such as the existence or otherwise of a crumpling transition remain unanswered and numerical simulation has played a large part in providing our present understanding. In practice nearly all the numerical results are obtained on surfaces embedded in $D = 3$ dimensions.

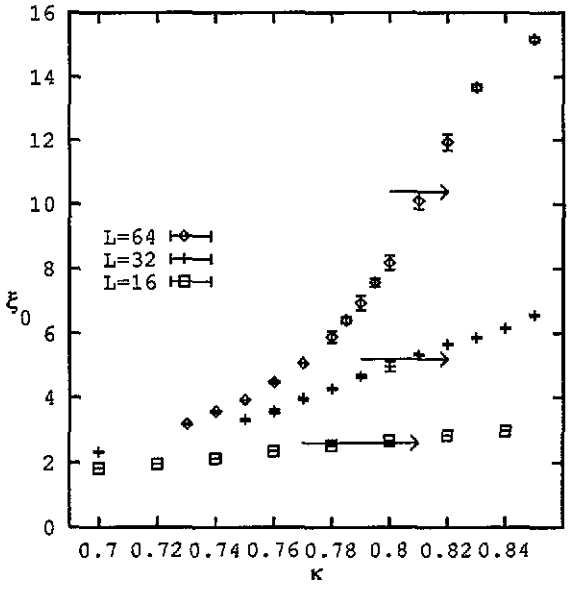

Figure 8. The zeroes of the crystalline surface correlation function $G_\parallel$ as a function of κ for different lattice sizes.

As discussed in section 5.3 the tangent–tangent correlation functions yield a great deal of information about the system. Since $G_\parallel(\xi)$ must become negative at large ξ, $G_\parallel(\xi_0) = 0$ for some ξ_0. Supposing the model has only one relevant length scale, the mass gap in the crumpled phase, m, satisfies

$$m \propto \xi_0^{-1} \tag{68}$$

on an infinite size system. However, on a finite size system with L lattice spacings in the 1 direction the value of ξ_0 cannot exceed $L/4$ [22] and when the ξ_0 appropriate to $L \to \infty$ approaches $L/4$ we expect to see finite-size effects. Figure 8 shows ξ_0 extracted

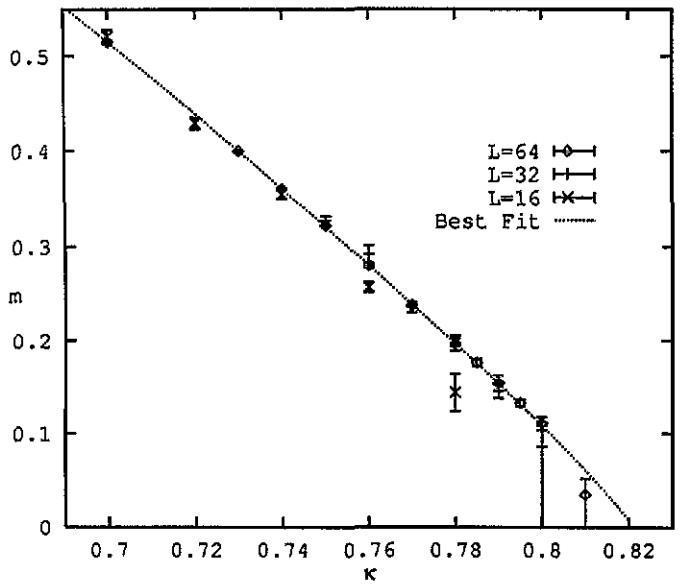

Figure 9. The mass gaps deduced from the data in figure 8 by using (69) to analyse the finite size effects.

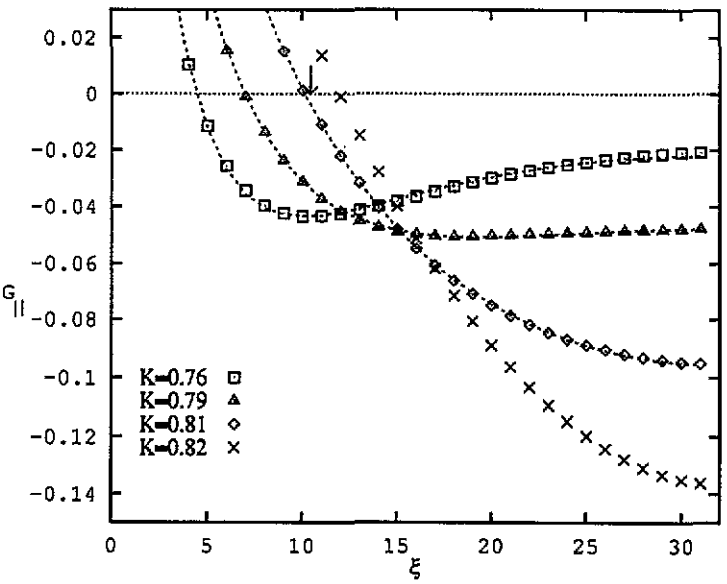

Figure 10. The crystalline surface correlation function $G_{\|}$ at large distances for different κ values on a 64^2 lattice. The broken lines show a fit of the form of (69).

from measured correlation functions $G_{\|}$ on 16^2, 32^2 and 64^2 systems and clearly illustrates the existence of these finite-size effects [36]. To unravel them requires some model; it has been known for some time [22] that the correlation functions in the crumpled phase are well described at long distances by supposing that the system is essentially a free-field theory and that in momentum space

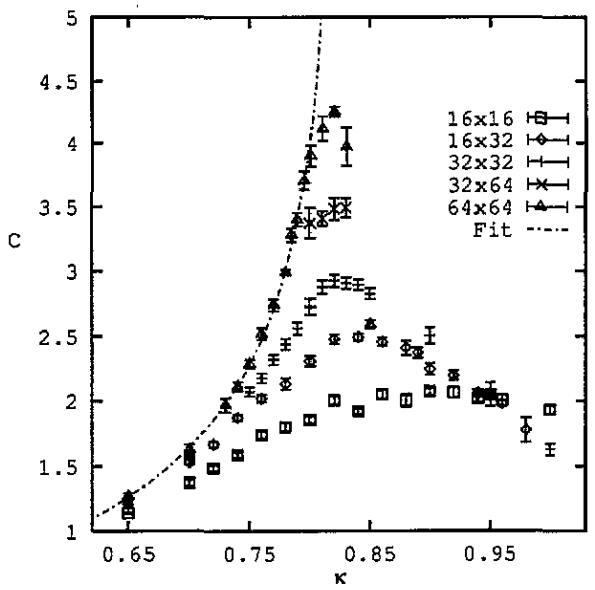

Figure 11. The specific heat of the crystalline surface as a function of κ for different lattice sizes. The line is the best fit of (72) to the 64^2 results.

$$\langle \boldsymbol{X}(\vec{p}) \cdot \boldsymbol{X}(-\vec{p}) \rangle \propto \frac{1}{L(\vec{p})(L(\vec{p}) + m^2)} \tag{69}$$

where $L(\vec{p})$ is the lattice Laplacian. Fitting (69) to the data in the region where $G_\parallel \leqslant 0$ yields the values of m shown in figure 9. Provided ξ_0 is far enough away from $\xi_0^{\max}$, the values obtained from the different lattices merge and are seen to be in very good agreement. The correlation length exponent ν is found by fitting by the usual form

$$m \sim (\kappa_c - \kappa)^\nu \tag{70}$$

which gives $\nu = 0.89 \pm 0.07$ and $\kappa_c = 0.821 \pm 0.005$. More information can be extracted from the correlation functions. Figure 10 shows $G_\parallel$ on a 64^2 lattice in the region where it is negative together with the best fit of (69) for a number of κ values close to the transition. At large enough distances, the correlation functions are dominated by the $L(\vec{p})^{-1}$ piece in (69) which leads to $G_\parallel \sim -\xi^{-2}$ implying that $\epsilon = 0$ in (50) and hence that for $\kappa < \kappa_c$, $d_H = \infty$. Up to $\kappa = 0.81$ the data is in very good agreement with this behaviour of $G_\parallel$ confirming that $d_H = \infty$ for $\kappa < \kappa_c$. The arrow shows $\xi_0^{\max}$ if the two point function takes the form of (69) and we see that the intercept for $\kappa = 0.82$ falls well beyond $\xi_0^{\max}$ and (69) no longer accounts for the long-distance behaviour of $G_\parallel$. That the two point function suddenly switches from following (69) to something completely different is really the most convincing single piece of evidence for the crumpling transition while the steady progression of m towards zero suggests that the transition is second order.

Complementary information is provided by the specific heat

$$C = \frac{1}{N}\left(\langle S^2 \rangle - \langle S \rangle^2\right) - \tfrac{3}{2} \tag{71}$$

which is shown in figure 11 for various lattice sizes [36]. The peak height grows steadily, and its location moves toward smaller κ, with increasing system size N, a classic indication of a second-order phase transition. The results for the 64^2 lattice are well fitted by the standard divergent behaviour

$$C = a + b(\kappa_c - \kappa)^{-\alpha} + \cdots \qquad \alpha = 0.2 \pm 0.15\,. \tag{72}$$

This implies that $\alpha - 2 + \nu d = 0.02 \pm 0.3$ in reasonable agreement with the scaling relation $\alpha = 2 - \nu d$.

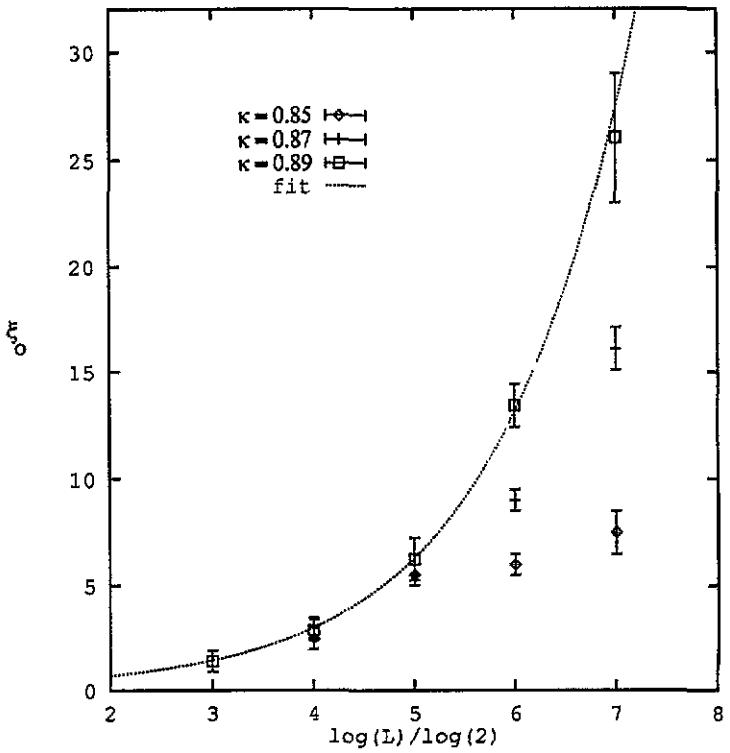

Figure 12. ξ_0 as a function of lattice size L for κ values in the vicinity of the transition. The broken curve shows the best fit to $\xi_0 \sim L^{1-\eta}$.

A finite-size scaling analysis of the specific heat assuming the scaling relation $\alpha = 2 - \nu d$ and the asymptotic behaviour

$$C_{\max} = a' + b' L^{\omega} + \cdots \tag{73}$$

where $\omega = \alpha/\nu$ and L is the linear size of the system gives a much larger value for α [36],

$$\alpha = 0.47 \pm 0.1 \qquad \nu = 0.76 \pm 0.05\,. \tag{74}$$

Other studies of this kind [37, 40] have found $\nu = 0.78 \pm 0.02$ and $\nu = 0.6 \pm 0.2$ which is in fair agreement with [36]. However, these results seem to differ systematically from those obtained from the 64^2 lattice alone which does rather suggest that most of the small lattice data is not in the asymptotic regime.

It has been shown fairly conclusively that $d_H = 2$ in the smooth phase [22, 37]. This was done in two ways; firstly by examining $G_{\|}$ again and secondly by studying the N dependence of $\langle X^2 \rangle$.

Figure 12 shows the behaviour of n_0 with L for couplings close to the phase transition [22]. (Unfortunately this simulation was done a different way to the others and there is an *a priori* unknown renormalization between the coupling constants so that here the critical coupling is about 0.88.) It is clear from the picture that there is a dramatic change in behaviour around $\kappa = 0.87$. Below this coupling n_0 seems to be saturating as L increases—precisely what we expect in the crumpled phase. On the other hand, at $\kappa = 0.89$ the steady growth of n_0 without apparent limit contrasts strongly with the behaviour at smaller

couplings. Of course this does not prove the continued growth for arbitrary L but it can be analysed according to (54) to provide an estimate for d_H. A fit of $n_0 \sim L^{1-\eta}$ (which is the dotted curve in figure 12) gives a best value of $\eta = -0.06$ with $\eta = 0.07$, 0.13 at one and two standard deviations and hence

$$d_H < 2.07 \text{ or } 2.14 \tag{75}$$

at one and two standard deviations respectively. This is fairly good evidence that the system jumps to $d_H = 2$ at the crumpling transition.

The alternative method is to fit measured values of $\langle X^2 \rangle$ to the form

$$\langle X^2 \rangle = aN^{2/d_H}. \tag{76}$$

This was done for κ values just in the smooth phase by [22] on $N = 32^2, 64^2, 128^2$ giving the estimate $d_H = 2.1$ and by [37] on $N = 8^2, 12^2, 16^2, 24^2, 32^2$ giving $d_H < 2.38$. Thus the behaviour of $\langle X^2 \rangle$ clearly supports the conclusion that $d_H = 2$ in the smooth phase.

It is not clear that the critical point is governed by a conformally invariant theory. The results for the long-distance behaviour of the correlation functions [36] suggest that the effective action might take the form

$$S_{\text{eff}} = \int -1/2m(\kappa)^2 \boldsymbol{X} \cdot \Delta \boldsymbol{X} + \boldsymbol{X} \cdot \Delta^2 \boldsymbol{X} \, \mathrm{d}^2\xi \tag{77}$$

where Δ is the Laplacian. This action is not classically or quantum mechanically conformally invariant. However, there may be corrections to (77) in the form of interaction terms which existing numerical simulations are not accurate enough to pick up. Whether a theory is conformally invariant or not it is always possible to look for finite-width behaviour for the free energy of the form

$$f = f_\infty + \frac{Ac}{L}. \tag{78}$$

If the theory *is* conformally invariant then A is a computable constant which depends only on the boundary conditions, c is the central charge and L is the strip width [38]. If the theory is *not* conformally invariant then one may still observe behaviour of the form (78) but c will not be the central charge; on the other hand entirely different behaviour such as $L^{-1/2}$ might be observed. If the effective action at κ_c is precisely given by (77) then it is easy to calculate f analytically and find that it does behave according to (78) with $c = 2D$. On the other hand, [39, 40] have measured f directly and find behaviour consistent with (78) but with c lying between zero and one. Whether or not the critical point is conformally invariant there is an apparent inconsistency here. The most likely resolution is simply that (77) is not exact but that there are interaction terms as well; it is certainly the case that more work needs to be done before the exact nature of the crumpling transition is identified.

When self avoidance is introduced the crumpling transition for tethered surfaces (6) [41] and for the model considered here [42] disappears for $D = 3, 4$; the surface has $d_H = 2$ for all values of κ and there is no critical behaviour. However, when $D = 5$ it has been found that the crumpling transition reappears [43]! This is remarkably close to the upper critical dimension $D_{uc} = 4.98$ predicted by the calculation of [35]. The absence of a diverging correlation length for $D = 3, 4$ makes the construction of a continuum limit impossible and so the models appear not to be suitable discretizations of continuum surfaces; on the other hand, as descriptions of possible real crystalline membranes they are perfectly in order.

6. The fluid surface

6.1. Analytic calculations

A large-D continuum calculation, analogous to that for the crystalline surface described in section 5.4, can be done for the fluid surface [29,44]. The difference is that there is no longer the fixed-area constraint (32) and instead there is an additional functional integral over the metric degree of freedom g. In the conformal gauge $g_{ab} = \delta_{ab}e^{\phi}$ where ϕ is often called the Liouville field. Schematically we get, after integrating out the X fields

$$Z = \int \mathrm{D}\lambda\, \mathrm{D}\phi \exp\{-DS_{\mathrm{eff}}(\lambda, \phi)\}\,. \tag{79}$$

As $D \to \infty$ the integral can be evaluated by the saddle-point technique and a translation invariant ansatz $\lambda(\vec{\xi}) = \lambda^0$, $\phi(\vec{\xi}) = \phi^0$ is made to minimize S_{eff}. This leads to the beta function

$$\beta(\alpha) = \frac{D}{4\pi}\alpha^2 + \cdots \qquad \alpha = \frac{1}{\kappa} \tag{80}$$

(recall that S_{eff} already depends on an ultra-violet cut-off because the X fields have been integrated out). Corrections to this approximation are obtained by integrating over small fluctuations in ϕ and λ. David and Guitter [45] showed that for surfaces with small enough physical string tension the matrix of second derivatives

$$\begin{pmatrix} \dfrac{\delta^2 S_{\mathrm{eff}}}{\delta\lambda(\vec{\xi})\delta\lambda(\vec{\xi}\,')} & \dfrac{\delta^2 S_{\mathrm{eff}}}{\delta\lambda(\vec{\xi})\delta\phi(\vec{\xi}\,')} \\ \dfrac{\delta^2 S_{\mathrm{eff}}}{\delta\phi(\vec{\xi})\delta\lambda(\vec{\xi}\,')} & \dfrac{\delta^2 S_{\mathrm{eff}}}{\delta\phi(\vec{\xi})\delta\phi(\vec{\xi}\,')} \end{pmatrix} \tag{81}$$

necessarily has some negative eigenvalues if $D > 1$ so that the integral over small fluctuations is infinite. The instability is associated with the presence of the Liouville field; this is a generic problem in string theories at $\kappa = 0$ where the kinetic term in the effective action for ϕ becomes negative if D is large enough. In the present case the result tells us that the true ground state of the system at large D breaks translational invariance and is presumably very complicated; it is tempting to suppose that the problem is related to the appearance of the branched polymer configurations which are discussed in the next section.

It has long been held [9] that the absence of massless 'phonon' modes (see section 5.4) in the fluid surface means there is no possibility of evading the Mermin–Wagner theorem and hence no phase transition at finite κ (so the beta function (80) is always asymptotically free unlike the crystalline membrane case). At long distance scales the extrinsic curvature term becomes irrelevant no matter what the value of α_0 and the surface is always crumpled. However, we will shortly see that the results of numerical simulation of the DTRS are not so unequivocal.

6.2. Thermodynamic limit of the DTRS and the string exponent

The most basic result is the existence of the grand canonical partition function (12) for large enough μ. Exploiting the fact that S_{ec} is bounded and that (on a torus) the number of links is three times the number of points we get immediately that

$$Z(\mu, \kappa, \beta) < Z(\mu - 6\kappa, 0, \beta)\,. \tag{82}$$

Integrating out the Xs we obtain

$$\mathcal{Z}(\mu, 0, \beta) = \sum_N \mathrm{e}^{-\mu N} \beta^{-(N-1)D/2} \sum_{T \in T_N} \left(\det{}' I_T\right)^{-D/2} \tag{83}$$

where I_T is the incidence matrix of T and $\det'$ indicates that the zero eigenvalue is suppressed. It is a standard result that $\det' I_T$ is equal to the number of spanning trees † that can be drawn on the graph T and is therefore greater than or equal to one. The number of triangulations in T_N is known to be bounded by e^{aN} for some constant a [46] and hence

$$\mathcal{Z}(\mu, 0, \beta) \leqslant \sum_N \mathrm{e}^{-\mu N} \beta^{-(N-1)D/2} \mathrm{e}^{aN} . \tag{84}$$

It immediately follows that by choosing μ large enough the sum over N can be rendered finite.

The divergence of $\mathcal{Z}$ as μ decreases to its critical value $\mu_c(\beta, \kappa)$ is parametrized by an exponent γ_{str} which controls the approach to the thermodynamic limit. Writing

$$\mathcal{Z}(\mu, \kappa, \beta) = \sum_N \mathrm{e}^{-\mu N} Z(\kappa, \beta, N) \tag{85}$$

we suppose the asymptotic behaviour

$$Z(\kappa, \beta, N) \sim N^{-2+\gamma_{\mathrm{str}}} \mathrm{e}^{bN} \tag{86}$$

which leads to the result that the expected number of points in the surface diverges as

$$\langle N \rangle \sim (\mu - \mu_c)^{-\gamma_{\mathrm{str}}} . \tag{87}$$

This exponent is important for at least two reasons. Firstly, unlike the critical free energy density μ_c, it is believed to be a universal quantity; its value is determined only by the universality class of the dynamics. The second reason is that it can be argued that on a manifold of arbitrary topology γ_{str} depends on the Euler characteristic χ_E of the manifold through

$$\gamma_{\mathrm{str}}(\chi_E) = \frac{\chi_E}{2} \gamma_{\mathrm{str}}(0) + 2 - \chi_E \tag{88}$$

whereas μ_c is independent of topology. Thus the exponent controls the behaviour of the system when a sum over topology (which defines string perturbation theory and is presumably necessary in a full theory of quantum gravity) is included [47]. In the case of $c < 1$ conformal matter coupled to the random triangulations these results are known to be true and the value of $\gamma_{\mathrm{str}}(0)$ is computable [31, 48],

$$\gamma_{\mathrm{str}}(0) = \tfrac{1}{12}\left(c - 1 - \sqrt{(25-c)(1-c)}\right) . \tag{89}$$

Note that this result depends only upon c, confirming its universal nature, and that it fails if $c > 1$ yielding a complex exponent. The reason for the failure is that a self-consistent

† A spanning trees is a connected set of links such that every site is visited and that there are no closed loops.

calculation has picked the wrong ground state. At present no analytical method of calculating for $c > 1$ is known; some effort has been made to measure γ_{str} for the DTRS when $\kappa = 0$ [49] but, apart from a rigorous upper bound of $\frac{1}{2}$ [4], little is known about it in the more interesting $\kappa > 0$ region.

There is one other observation that follows from (83) concerning the dominant configurations in the partition function for small κ. As D increases, those configurations with the smallest $\det' I_T$ become more important provided there are a significant number of them. One such configuration is the branched polymer of which an example is shown in figure 13; the tubes are typically only a few links in circumference. It is intuitively clear that such a triangulation has a relatively small number of spanning trees and hence a small determinant and it is also clear that there is a very large number of distinct branched polymers. The value of D where these configurations start to dominate is unknown but it is tempting to suppose that $D = 1$ is the critical value and that the onset of branched-polymer dominance coincides with the failure of KPZ (see [50] for a more detailed discussion). As we discussed briefly in the continuum context in section 3, the hope is that the extrinsic curvature will suppress these very far from smooth surfaces at large enough values of κ.

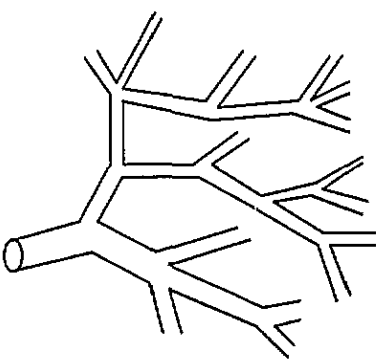

Figure 13. A branched polymer configuration.

6.3. Correlation functions

In section 4 we saw how the study of correlation functions and extraction of the mass gap and string tension is crucial to understanding the properties of the system. The mass gap and string tension are defined in the grand canonical ensemble but some analysis is much more straightforward in the canonical ensemble, as is numerical simulation. It is therefore convenient to express them in terms of quantities measurable in the canonical ensemble [51]. In the following we will denote by V_d a d-dimensional boundary of volume V_d (so that for G_1 we have $V_d = A$ and for G_2, $V_d = L$); the boundary will contain n fixed points and the rest of the surface $N - 1$ points that are free to move. The Gibbs free energy $\mathcal{G}$ and the Helmholtz free energy F are related by

$$e^{-\mathcal{G}(\mu,\kappa;V_d)} = \sum_N e^{-\mu N} e^{-F(\kappa,N;V_d)} \tag{90}$$

from which we get

$$\langle N \rangle = \frac{\partial \mathcal{G}(\mu, \kappa; V_d)}{\partial \mu}\Big)_{\kappa, V_d} \tag{91}$$

and

$$\frac{\partial \mathcal{G}(\mu, \kappa; V_d)}{\partial V_d}\Big)_{\mu,\kappa} = \left\langle \frac{\partial F(\kappa, N; V_d)}{\partial V_d}\Big)_{\kappa,N} \right\rangle \tag{92}$$

where the expectation is in the grand canonical ensemble. In the thermodynamic limit we make a saddle-point expansion for the sum over N and find that to leading order in its location, $\overline{N}$,

$$\langle N \rangle = \overline{N}$$

$$\left\langle \frac{\partial F(\kappa, N; V_d)}{\partial V_d}\Big)_{\kappa,N} \right\rangle = \frac{\partial F(\kappa, \overline{N}; V_d)}{\partial V_d}\Big)_{\kappa,\overline{N}}. \tag{93}$$

Differentiating (24) and (25) with respect to A and L respectively this result relates the string tension and the mass gap to quantities measurable in the canonical ensemble by

$$\sigma(\mu, \kappa) = \frac{\partial F(\kappa, \overline{N}; A)}{\partial A}\Big)_{\kappa,\overline{N}} \qquad \overline{N} = A\frac{\partial \sigma(\mu, \kappa)}{\partial \mu}\Big)_{\kappa} \tag{94}$$

and

$$m(\mu, \kappa) = \frac{\partial F(\kappa, \overline{N}; L)}{\partial L}\Big)_{\kappa,\overline{N}} \qquad \overline{N} = L\frac{\partial m(\mu, \kappa)}{\partial \mu}\Big)_{\kappa}. \tag{95}$$

Now consider the canonical ensemble with some d-dimensional boundary of d-volume V_d. The partition function is given by

$$Z(\kappa, \beta, N; V_d) = \sum_T \prod_{i=1}^{N+n-1} \int \mathrm{d}^D \boldsymbol{X}(i)\, \mathrm{e}^{-(\beta S_G + \kappa S_{ec})} C(\boldsymbol{X}(1), \ldots, \boldsymbol{X}(n); V_d) \tag{96}$$

where C imposes the boundary constraints on the n boundary points. Rescaling all the $\boldsymbol{X}$s by $\boldsymbol{X} \to \lambda \boldsymbol{X}'$ and exploiting the scale invariance of S_{ec} we find

$$Z(\kappa, \beta, N; V_d) = \lambda^{(N-1)D} Z(\kappa, \lambda^2 \beta, N; \lambda^{-d} V_d). \tag{97}$$

Differentiating the logarithm of this relation with respect to λ and putting $\lambda = 1$, $\beta = 1$ yields

$$0 = (N-1)D - 2\langle S_G \rangle + \mathrm{d}V_d \frac{\partial}{\partial V_d} F(\kappa, N; V_d) \tag{98}$$

whence ($d = 2$)

$$\sigma(\kappa, N, A) = \frac{2\langle S_G \rangle - (N-1)D}{2A} \tag{99}$$

and ($d = 1$)

$$m(\kappa, N, L) = \frac{2\langle S_G \rangle - (N-1)D}{L} \tag{100}$$

and ($d = 0$)

$$\langle S_G \rangle = (N-1)\frac{D}{2}. \tag{101}$$

It is now straightforward to prove that at $\kappa = 0$ the string tension is non-zero (this was originally proved in the grand canonical ensemble [52] but here we use the canonical ensemble). Consider the canonical ensemble with boundary loop of area A and let $X(i) = X^0(i) + x(i)$ where $X^0(i)$ is that location of the site i which minimizes S_G on the particular triangulation T. Then

$$S_G = \min(S_G) + \sum_{\langle ij \rangle} (x(i) - x(j))^2 \tag{102}$$

and, because $X(i) = X^0(i)$ on the boundary points by definition, $x(i) = 0$ if i is a boundary point. Now the sum of the squares of the length of any two sides of a triangle is greater than four times its area so

$$\min(S_G) \geqslant 2A. \tag{103}$$

The remaining ensemble defined by the xs has $V_d = 0$ so, by (101),

$$\langle S_G \rangle \geqslant 2A + (N-1)\frac{D}{2} \tag{104}$$

whence

$$\sigma \geqslant 2. \tag{105}$$

Extending the argument to positive κ introduces an extra term in (104) which is negative and hence, as was shown in [53], it is possible to get $\sigma = 0$ for some $\kappa = \kappa_c \neq 0$.

The situation for the mass gap is different. Following the same argument as above we again need to evaluate $\min(S_G)$. It is obvious that this will occur when all points collapse onto the straight line joining the two boundary points. There is a tube-like triangulation whose circumference is just three links for which the average link length is $\sim L/N$ and hence

$$\min(S_G) \approx N\left(\frac{L}{N}\right)^2 = L\left(\frac{L}{N}\right). \tag{106}$$

In the thermodynamic limit $N \to \infty$ and hence $m \to 0$. We expect this behaviour to persist for increasing κ at least until any phase transition is reached.

We have seen that in order for $m, \sigma \to 0$ it is necessary (but not necessarily sufficient) to have $\kappa > 0$. Unfortunately, it is much more difficult to prove that, for $\kappa \to \kappa_c$, the mass gap and string tension vanish such that σ/m^2 tends to a constant. There are no analytic results available on this point and such information that we have comes from numerical simulations. In order to interpret the results of the numerical simulations that we will discuss in the next section it is useful to consider the possible scaling behaviour of the mass gap and the string tension [51]. In the thermodynamic limit, where $\mu \to \mu_c(\kappa)$, we expect

$$\sigma(\mu, \kappa) = \sigma_0(\kappa) + d(\kappa)(\mu - \mu_c(\kappa))^{2\nu(\kappa)} \tag{107}$$

where $\sigma_0(\kappa)$ might vanish at κ_c and $d(\kappa)$ is a regular function. Supposing that the string tension *does* vanish somewhere then, in order to get $\sigma/m^2 \to$ const in the thermodynamic limit, we need

$$m(\mu, \kappa) = e(\kappa)(\mu - \mu_c(\kappa))^{\nu(\kappa)} \tag{108}$$

where $e(\kappa)$ is a regular function. Using (94) and (95) we can relate this behaviour to the canonical ensemble and obtain

$$\sigma(\kappa, N) = \sigma_0(\kappa) + d(\kappa)\left(\frac{A}{N}\right)^{2\nu(\kappa)/(1-2\nu(\kappa))} \tag{109}$$

and

$$m(\kappa, N) = e(\kappa)\left(\frac{L}{N}\right)^{\nu(\kappa)/(1-\nu(\kappa))} . \tag{110}$$

The results (109), (110) tell us how the string tension and mass gap measured in the canonical ensemble using (99), (100) are expected to scale in the thermodynamic limit if there is a non-trivial critical point.

6.4. Numerical simulation

The numerical simulations provide information about bulk quantities such as the specific heat and the behaviour of loop correlation functions which determine the mass gap and the string tension. The difficulties associated with simulating the dynamically triangulated systems are formidable. Earlier simulations [54–56] suggested that there is a crumpling transition similar to that in the crystalline surface but as larger system sizes have beeen studied the transition has become weaker. The largest system sizes that have been studied, $N = 2304$, are smaller than for crystalline surfaces. This alone makes the identification of finite-size effects and extraction of the infinite volume limit more difficult.

Four recent papers have reported results for the bulk thermodynamic quantities which are in broad agreement although there is some spread in the location of the peak in the specific heat [51, 57–59]. As for the crystalline surface, the internal energy of the system is continuous and there is no evidence for a first-order transition. Figure 14 (which is taken from [51] whose λ is the same as our κ) shows the specific heat which displays a peak at $\kappa \approx 1.4$. However, the nature of the peak is very different from the crystalline case because, although it grows rapidly with N for small lattices ($N \leqslant 144$), at larger N values the growth abates and there is no evidence that the peak height diverges as $N \to \infty$; indeed the results of [59] show that the peak height has saturated at $N = 576$. There is insufficient data even to fit the asymptotic behaviour of C_{max} to (73) and fits of the standard divergent behaviour are impossible leaving us with the likelihood that $\alpha < 0$ which would account for cusp-like behaviour of C but no more definite information.

Figure 15 shows the string tension, measured in a simulation using (99) at several κ values, plotted against A/N [51]. When κ is well below the region where the peak in the specific heat occurs it seems clear that the string tension is tending towards a finite value as $A/N \to 0$. However, as κ increases the limiting value is getting smaller and at $\kappa = 1.5$ there is no evidence that the curve is flattening out for the values of A/N at which measurements were possible. The data points in figure 15 also show a steady progression

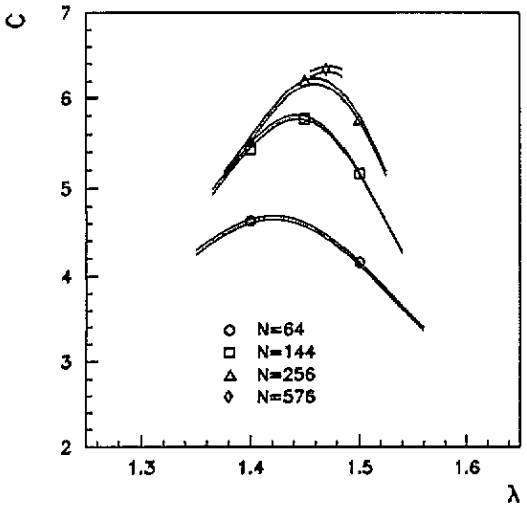

Figure 14. The specific heat of the DTRS as a function of $\lambda\,(=\kappa)$ for different lattice sizes [51]. It appears not to be diverging as the system size increases.

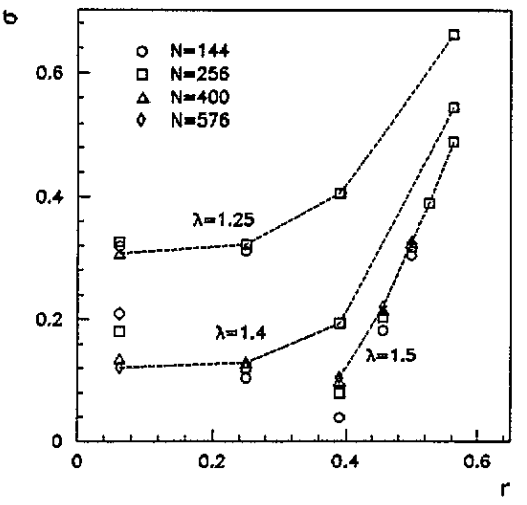

Figure 15. The string tension of the DTRS plotted against $r = A/N$ for different $\lambda\,(=\kappa)$ values and various system sizes [51].

in σ at fixed A/N as N increases which allows the finite-size effects to be controlled by extrapolating $N \to \infty$ at fixed A/N. Using (109) the exponent ν is estimated to be

$$0.38 < \nu(\kappa = 1.5) < 0.42\,. \tag{111}$$

Figure 16 shows the mass gap, measured in a simulation using (100), plotted against L/N at the same κ values. This time we see that, as expected from (110), m appears to be falling to zero as $L/N \to 0$ no matter what the value of κ. Fitting (110) to the data at $\kappa = 1.5$ yields $\nu = 0.417 \pm 0.007$ which is within the range implied by the string tension results (111); accordingly the simulation data is consistent with the ratio σ/m^2 being finite. However, it should be borne in mind that these string tension measurements were made on lattices of $N = 576$ and smaller; this is precisely the lattice size at which the specific heat saturates and maybe σ saturates at a finite value too.

Measurements of R_g^2 suggest that in the critical region

$$R_g^2 \sim N^{2/d_H} \tag{112}$$

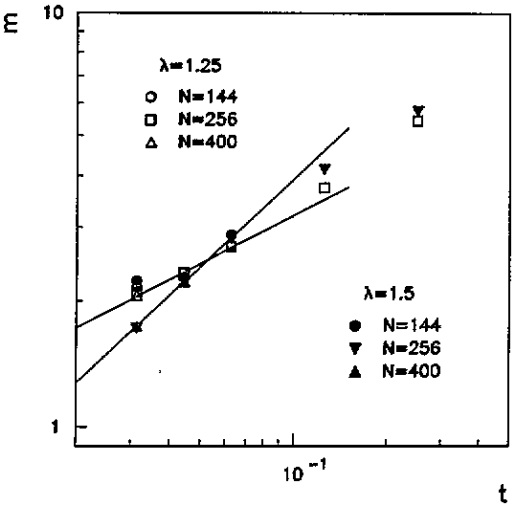

Figure 16. The mass gap of the DTRS plotted against $t = L/N$ for different λ ($= \kappa$) values and various system sizes [51].

with $d_H > 3.4$ [51] or $d_H \sim 4$ [57]. Unfortunately, this is consistent with the dominant configurations being the branched polymers discussed in section 6.2 and it remains to be seen if a genuine smooth surface is obtained at κ_c.

The latest numerical data is consistent with there being a phase transition at $\kappa \approx 1.5$ and with both σ and m vanishing at the transition with a finite ratio σ/m^2. However, the evidence for the transition is nowhere near as conclusive as for the crystalline surface. The situation is complicated by the fact that, if the transition does exist, it must surely be third (or higher) order and the existing data is too sparse for a precise study of such a phenomenon. It has also been pointed out by [57] that the results look suspiciously similar to those obtained in other lattice field theory models which are known to have cross-overs rather than genuine phase transitions.

The effects of self-avoidance have also been studied for the DTRS [42, 60]. Unlike those of the crystalline membrane the critical properties of the DTRS (if that is what they are) seem to survive the introduction of self-avoidance but again the very small lattices involved leave the interpretation of the results open to doubt.

7. In closing

The existence of a crumpling transition in the crystalline surface is well established. However, there is as yet no first principles proof of this, we still do not know the critical exponents very accurately and there is considerable uncertainty over the properties of the effective field theory at the critical point. The difficulties are compounded by the fact that the model is, at least naively, non-unitary because of the higher derivative terms in the kinetic part of the action and less is known about the classification of non-unitary conformal field theories in two dimensions. From the numerical point of view further progress could probably be made by renormalization-group studies of the model and the availability of ever more powerful computers. Nonetheless, progress would undoubtedly be made more quickly if the conceptual framework for these transitions were clearer.

In the case of the fluid surface it is still not clear whether there is a phase transition at all, let alone its detailed features. If there is in fact no transition then a continuum string (or string-like object) embedded in $D = 3$ dimensions is probably impossible without

introducing fermionic degrees of freedom into the problem. A rigorous proof that the string tension does, or does not, vanish at a finite value of κ would be a big step forward.

Acknowledgments

I am grateful to J Ambjørn, D Espriu and T Jonsson for many illuminating discussions, to the authors and publishers of [51] for permission to reproduce figures 14–16 and to the publishers of [22, 36] to reproduce material.

References

[1] Nambu Y 1970 *Lectures at the Copenhagen Summer Symposium*
[2] Mandelstam S 1974 *Phys. Rep.* C **13** 259
[3] Polyakov A M 1981 *Phys. Lett.* **103B** 207
[4] Ambjørn J, Durhuus B and Fröhlich J 1985 *Nucl. Phys.* B **257** [FS14] 433
[5] David F 1985 *Nucl. Phys.* B **257** [FS14] 543
[6] Kazakov V A, Kostov I K and Migdal A A 1985 *Phys. Lett.* **157B** 295
[7] Helfrich W 1973 *Z. Naturforsch.* C **28** 693
[8] Helfrich W 1985 *J. Phys.* 46 1263
[9] Peliti L and Leibler S 1985 *Phys. Rev. Lett.* **54** 1690
[10] Foerster D 1986 *Phys. Lett.* **114A** 115
[11] Casher A, Foerster D and Windey P 1985 *Nucl. Phys.* B **251** [FS13] 29
[12] Sterling T and Greensite J 1983 *Phys. Lett.* **121B** 345
Maritan A and Stella A L 1984 *Phys. Rev. Lett.* **53** 123
[13] Migdal A A 1983 *Phys. Rep.* **102** 199
[14] R K P Zia 1985 *Nucl. Phys.* B **251** 676
[15] Nelson D, Piran T and Weinberg S (eds) 1989 *Statistical Mechanics of Membranes and Surfaces* (Singapore: World Scientific)
[16] Gross D J, Piran T and Weinberg S (eds) 1992 *Two-Dimensional Quantum Gravity and Random Surfaces* (Singapore: World Scientific)
[17] David F Simplicial quantum gravity and random lattices *Saclay Physique Theorique preprint* 93/028
[18] Baumgartner A 1993 *J. Chem. Phys.* **98** 7496
[19] Kantor Y and Nelson D 1987 *Phys. Rev. Lett.* **58** 2774; 1987 *Phys. Rev.* A **36** 4020
[20] Espriu D 1987 *Phys. Lett.* **194B** 271
[21] Baig M, Espriu D and Wheater J F 1989 *Nucl. Phys.* B **314** 609
[22] Harnish R G and Wheater J F 1991 *Nucl. Phys.* B **350** 861
[23] Durhuus B and Jonsson T 1992 *Phys. Lett.* **297B** 3326
[24] Baillie C F, Espriu D and Johnston D A Steiner Variations on Random Surfaces *Colorado Preprint* COLO-HEP-297
[25] Espriu D and Baig M 1993 *Nucl. Phys.* B (Proc. Suppl.) **30** 779
[26] Ambjørn J, Durhuus B and Jonsson T 1989 *Nucl. Phys.* B **316** 526
[27] Nelson D R and Peliti L 1987 *J. Physique* **48** 1085
David F, Guitter E and Peliti L 1987 *J. Physique* **48** 2059
[28] David F and Guitter E 1988 *Europhys. Lett.* 5 709
[29] Polyakov A M 1986 *Nucl. Phys.* B **268** 406
[30] Weingarten D 1982 *Nucl. Phys.* B **210** [FS6] 229
[31] Knizhnik V G, Polyakov A M and Zamolodchikov A B 1988 *Mod. Phys. Lett.* A **3** 819
[32] Kantor Y and Jaric M V 1990 *Europhys. Lett.* **11** 157
[33] Jonsson T 1989 *Phys. Lett.* **221B** 35
[34] Pisarski R D 1983 *Phys. Rev.* D **28** 2547
[35] Le Doussal P and Radzihovsky L 1992 *Phys. Rev. Lett.* **69** 1209
[36] Wheater J F and Stephenson P W 1993 *Phys. Lett.* **302B** 447
[37] Renken R L and Kogut J B 1990 *Nucl. Phys.* B **342** 753
[38] Cardy J L 1990 *Fields, Strings and Critical Phenomena* ed E Brézin and J Zinn-Justin (Amsterdam: North-Holland)

[39] Renken R L and Kogut J B 1991 *Nucl. Phys.* B **348** 580
[40] Petersson B 1993 *Proc. Lattice 93 Conf. Nucl. Phys.* B (Proc. Suppl.) to appear
[41] Abraham F F, Rudge W E and Plishke M 1989 *Phys. Rev. Lett.* **62** 1757
Plishke M and Boal D 1989 *Phys. Rev.* A **38** 3292
Ho J-S and Baumgartner A 1989 *Phys. Rev. Lett.* **63** 1324
[42] Baillie C F and Johnston D A 1992 *Phys. Lett.* **283B** 55
[43] Grest G 1991 *J. Physique* **1** 1695
[44] Kleinert H 1986 *Phys. Lett.* **174B** 335
[45] David F and Guitter E 1988 *Nucl. Phys.* B **295** 332
[46] Tutte W T 1962 *Can. J. Math.* **14** 21
[47] Brézin E and Kazakov V A 1990 *Phys. Lett.* **236B** 144
Douglas M R and Shenker S H 1990 *Nucl. Phys.* B **335** 635
Gross D J and Migdal A 1990 *Phys. Rev. Lett.* **64** 127
[48] David F 1988 *Mod. Phys. Lett.* A **3** 1651
Distler J and Kawai H 1989 *Nucl. Phys.* B **321** 509
[49] Ambjørn J, Boulatov D and Kazakov V A 1990 *Mod. Phys. Lett.* A **5** 771
[50] Cates M E 1990 *Phys. Lett.* **251B** 553
[51] Ambjørn J, Jurkiewicz J, Varsted S and Irbäck A 1992 *Phys. Lett.* **275B** 295
Ambjørn J, Irbäck A, Jurkiewicz J and Petersson B 1993 *Nucl. Phys.* B **393** 571
[52] Ambjørn J and Durhuus B 1987 *Phys. Lett.* **188B** 253
[53] Ambjørn J, Durhuus B, Fröhlich J and Jonsson T 1987 *Nucl. Phys.* B **290** [FS20] 480
[54] Catterall S M 1989 *Phys. Lett.* **220B** 207
[55] Baillie C, Johnston D and Williams R 1990 *Nucl. Phys.* B **335** 469
Baillie C, Catterall S, Johnston D and Williams R 1991 *Nucl. Phys.* B **348** 543
[56] Renken R L and Kogut J B 1991 *Nucl. Phys.* B **354** 328
[57] Bowick M, Coddington P, Leping Han and Harris G 1993 *Nucl. Phys.* B **394** 791
[58] Münkel C and Heermann D W 1993 *Preprint* hep-th/9302025
[59] Anagnostopoulos K, Bowick M, Coddington P, Falcioni M, Leping Han, Harris G and Marinari E 1993 *Phys. Lett.* **317B** 102
[60] Ho J-S and Baumgartner A 1990 *Europhys. Lett.* **12** 295